

Morphology evolution of α phase in investment cast titanium matrix composites with B_4C additions

Jiheng Wang^{1,2} · Xianglong Guo¹ · Jining Qin¹ ·
Di Zhang¹ · Weijie Lu^{1,3}

Received: 1 January 2015 / Accepted: 20 May 2015 / Published online: 27 May 2015
© Springer Science+Business Media New York 2015

Abstract Titanium matrix composites were prepared by investment casting in a consumable arc skull casting furnace. With the addition of B_4C , the average primary β grains are refined, and the morphology of α phase tends to be more equiaxed. The free energy for nucleation consisting of the bulk free energy, orientation-independent interfacial energy, and elastic strain energy is calculated to investigate the role of nucleation sites in determining the shape of critical nucleus. In the current study, the TiB whiskers were found to be arranged in the grain boundary and provide heterogeneous nucleation sites for α precipitates, and the interfacial energy is about 14 % more than that in Ti-64, while its elastic strain energy is reduced to about three quarters of the latter one.

Introduction

Titanium matrix composites (TMCs) reinforced with ceramic particles have drawn great attention due to their considerable potential for significant improvements in both

mechanical properties and service temperature [1–6]. For years, in situ techniques, such as mechanical alloying, powder metallurgy, and solidification process, have been frequently developed to synthesize TMCs [7, 8]. Among various ways of producing TMCs, traditional ingot metallurgy plus self-propagation high-temperature synthesis reaction between titanium and B_4C has become a popular approach to produce TiB- and TiC-reinforced TMCs, due to a better interface between reinforcements/matrix and lower preparation cost [9, 10]. With B_4C additions, α precipitates mainly exhibit near equiaxed particles instead of the lamellar structure [11, 12]. Similar morphology was also reported in the work of Hill et al. [13] in a cast Ti-64 alloy with a small addition of boron. Though they mentioned that the formation of equiaxed α phases is relevant to the heterogeneous nucleation of α phases at TiB whiskers, no further explanation was proposed to clearly show the underlying physics of such morphology. In this study, the morphology evolution of α phase is studied experimentally and discussed theoretically in relation to the overall energy of the nucleation, inclusive of the α /TiB interfacial energy and elastic energy.

✉ Weijie Lu
luweijie@sjtu.edu.cn

¹ State Key Laboratory of Metal Matrix Composite, Shanghai Jiao Tong University, 800# Dongchuan Road, Shanghai 200240, People's Republic of China

² School of Material Science and Engineering, Jiangsu University of Science and Technology, 2# Mengxi Road, Zhenjiang 212003, People's Republic of China

³ Shanghai Key Laboratory of Advanced High-temperature Materials and Precision Forming, Shanghai Jiao Tong University, 800# Dongchuan Road, Shanghai, People's Republic of China

Materials and experiments

In this study, stoichiometric amounts of sponge titanium, B_4C , and alloying elements for synthesizing matrix Ti-6Al-4V (Ti-64) alloy were blended, and then melted in a vacuum consumable arc-melting furnace and cast into samples by investment casting in a consumable arc skull casting furnace. As comparison, matrix alloy without reinforcements was also prepared in the same way. The chemical composition of the matrix (similar to that of the α + β titanium alloy Ti-64) and the theoretical volume

fractions of TiB whiskers (obtained by calculating mathematical model of the reactants) are listed in Table 1.

Scanning electron microscope (SEM) samples were wire-cut from the cast samples and metallographically prepared by using conventional grinding and mechanical polishing techniques. The polished samples were etched with Kroll’s reagent. The microstructures were characterized by a FEI QUANTA-250 SEM. Transmission electron microscope (TEM) specimens with a diameter of 3 mm were prepared by grinding, dimpling, and twin-jet electro-polishing with a solution of 3 % perchloric acid and 97 % alcohol with temperature of 243–253 K, voltage of 65–75 V, and current of 30–40 mA. The TEM images and corresponding selected area diffraction (SAD) patterns were obtained by a Philips CM200 transmission electron microscope (TEM). The electron backscattered diffraction (EBSD) analysis was conducted in a FEI Quanta FEG 250 SEM equipped with EDAX/TSL OIMTM system. More than 250,000 points were acquired over an area of approximately 90,000 μm² for each EBSD map, and the average confidence index (CI) of them was ranged from 0.21 to 0.56. The specimens for EBSD studies were prepared by metallography and electro-polishing with a solution of 9 vol% perchloric acid, 91 vol% glacial acetic acid at 288 K. High-temperature X-ray diffraction (HTXRD) was employed to investigate the lattice parameters of phases at the temperature where nucleation occurs. The HTXRD specimen was wire-cut from the TMCs samples with a diameter of 16 mm, and the final sheet thickness is 0.8 mm after polishing. The diffraction experiments were carried out using an X’Pert PRO diffractometer (PW3040/60, Panalytical B.V., Netherlands) with a sample stage for Co anode (wavelength $k = 0.178897$ nm) and X-ray detector, operating at 40 kV and 40 mA, with a scanning speed of 0.15°/s over an angular range of 20°–90°. In these experiments, the sample was heated at a rate of 0.5 K/s when the sample reached the testing temperature holding for 480 s before scanning.

Results and discussions

Microstructure characterization

Figure 1 shows the SEM micrographs and distribution of the aspect ratio of α precipitates in Ti-64 alloy and TMCs. As seen in Fig. 1a, a typical widmanstatten structure forms

during investment casting when the alloys are solidified and cooled in a ceramic shell which reduces the cooling rate. The primary β grains are more than 1000 μm in size. When the Ti-64 alloy is slowly cooled down from a temperature above β solvus, α precipitates would firstly nucleate and grow along the previous β grain boundaries. Upon further cooling, parallel intergranular α plates nucleate from the β grain boundary, and grow into colony α phase with average thickness of 2.5 μm. In the present work, the aspect ratio of each α lath (surrounded by white lath boundaries) is defined as the ratio of its semi-major axis to the semi-minor axis. Statistic distribution of the aspect ratio of over 90 α laths in each sample is shown in Fig. 1b, which indicates that most α laths exhibit an aspect ratio smaller than 15, while some laths with larger aspect ratio (i.e., 16 and 21) still possess relatively high frequency. More detailed calculation suggests that in the Ti-64 alloy, 79 % of aspect ratios are distributed between 5 and 17 and the average aspect ratio of α lath is 13.8.

Compared with the Ti-64 alloy, the average size of primary β grains of TMCs is significantly reduced to 50–100 μm (Fig. 1c). Besides, the formation of Widmanstatten structure is eliminated in this case. It should be noted that white TiB whiskers, generated by eutectic reaction [14], form a necklace structure at the prior β grain boundaries, as shown in Fig. 1c. According to the reference materials [11, 15], the refinement of β grain size is due to the rejection of excess boron from β-Ti nuclei. In our study, the carbon content of the TMCs is 0.10 wt%, which is below the solid solubility of carbon of 0.126 wt% at 873 K [16, 17]. Therefore, the carbon will dissolve in β-Ti phases that nucleate from the liquid. However, the content of boron in TMCs is 0.38 wt%, which exceeds the solubility of boron value of 0.02 wt% at room temperature in titanium alloys [11]. Thus, extra boron is rejected from the primary β-Ti nuclei into the melt, and the composition of metal melt is changed. The change in the melt composition will cause a corresponding variation in the liquidus temperature and lead to higher constitutional super-cooling, which will enhance the nucleation rate and provide additional driving force and then reduce the growth rate of β-Ti [11, 18]. Furthermore, the precipitation of TiB whiskers between the β-Ti dendrites will interrupt the growth of β-Ti grain, and reduce the grain size. With the addition of B₄C, the morphology of α phase in TMCs tends to be more equiaxed than that of the Ti-64 alloy. About 80 % of aspect ratios are between 2 and 4 in TMCs as can be seen in

Table 1 Composition (wt%) and theoretical volume fractions (vol%) of reinforcements of Ti-64 and TMCs

Material	V	Al	B	C	Ti	volume fraction of TiB
Ti-64	4	6	0	0	Balance	0
TMCs	3.90	5.81	0.38	0.10	Balance	1.93

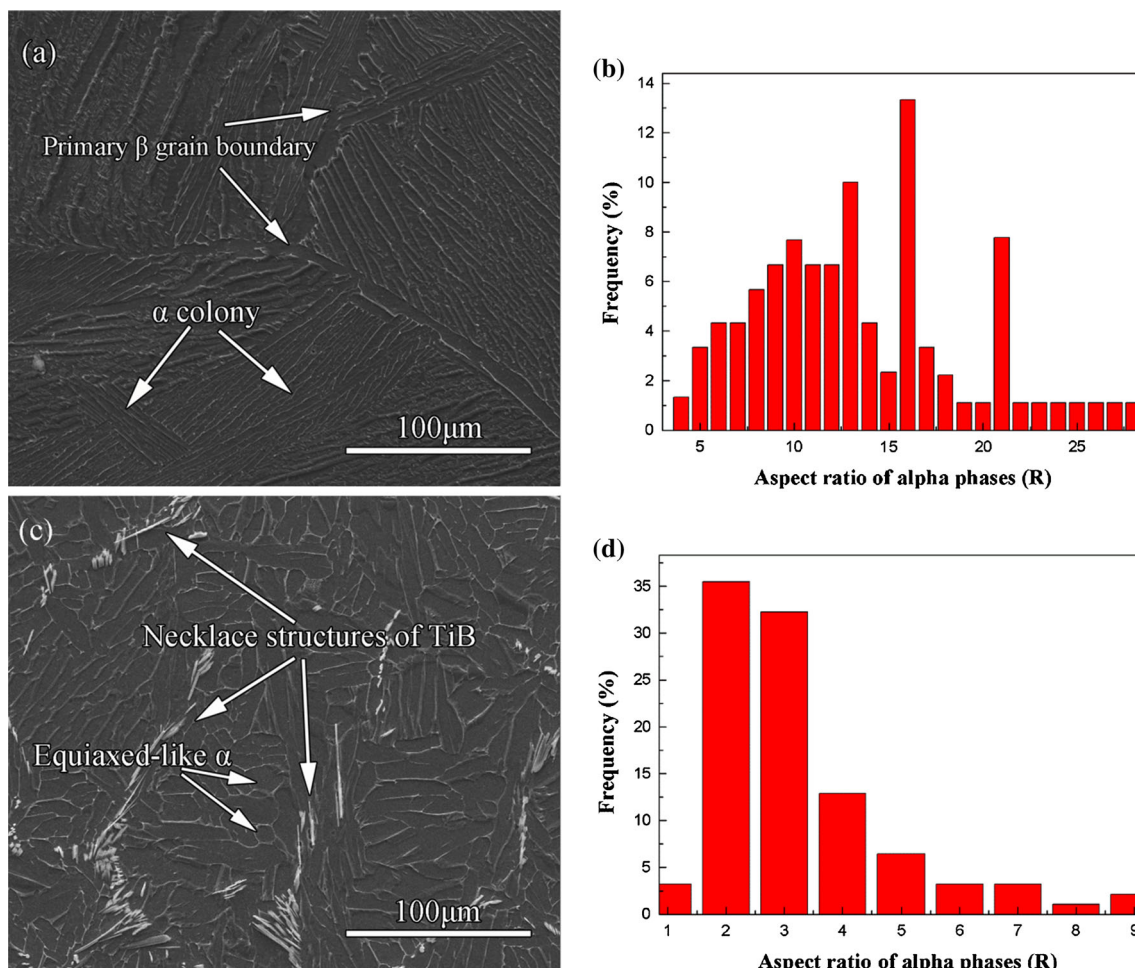


Fig. 1 Secondary electron imaging (SEI) and size distribution of the aspect ratio of investment cast samples: **a** SEI of Ti-64, **b** the distribution plot of the aspect ratio of α plate in Ti-64, **c** SEI of TMCs, **d** the distribution plot of the aspect ratio of α plate in TMCs

Table 2 Statistical analysis results of microstructural parameters of Ti-64 and TMCs

samples	Prior β grain size (μm)	Average aspect ratio of α (R)	Average aspect ratio of TiB (l/d)
Ti-64	>1000	13.8	–
TMCs	50–100	3.4	10.4

Fig. 1d. The average aspect ratio of α phases is 3.4 in TMCs. The statistical analyses of both Ti-64 and TMCs are summarized in Table 2 in order to clearly demonstrate the difference in the morphology of α precipitates. It should also be mentioned here that similar morphologies of TMCs have also been observed in boron-containing titanium alloys [11, 13, 19], indicating that TiB precipitates are responsible for the change of α morphology. To be specific, compared with the case of Ti-64 alloy where the initial nucleation of α precipitates takes place at prior β grain boundaries, the prior TiB whiskers could also offer additional nucleation sites for α precipitates.

More detailed morphology of α phase in both Ti-64 and TMCs is examined by TEM images. As can be seen in

Fig. 2a, the α phase in Ti-64 exhibits a typical lamellar structure. However, in TMCs, the α phase forms near the TiB whiskers, and presents a more equiaxed morphology which has a smaller aspect ratio, as shown in Fig. 2b. As also noted by Hill [13] that in most cases, shorter and thicker α precipitates (more equiaxed) are precipitated near the TiB whiskers.

Figure 3 shows the EBSD maps of Ti-64 alloy and TMCs. Figure 3a is the grain boundary map of Ti-64 which shows the different angle boundaries of α phases, in which the blue lines are high-angle ($\theta > 15^\circ$) boundaries, green lines are middle angle ($15^\circ > \theta > 5^\circ$) boundaries, and red lines are low-angle ($\theta < 5^\circ$) boundaries. The EBSD grain boundary map of Ti-64 shows a strong α colonies

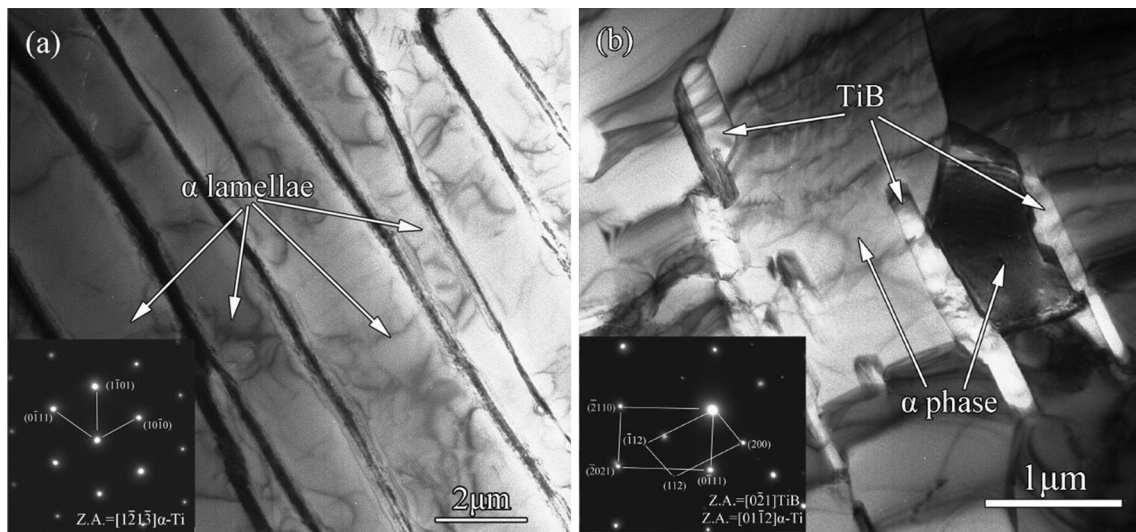


Fig. 2 Bright-field TEM micrographs of **a** α lamellae in Ti-64, **b** α phase in TMCs. Inserts show the corresponding SAD pattern

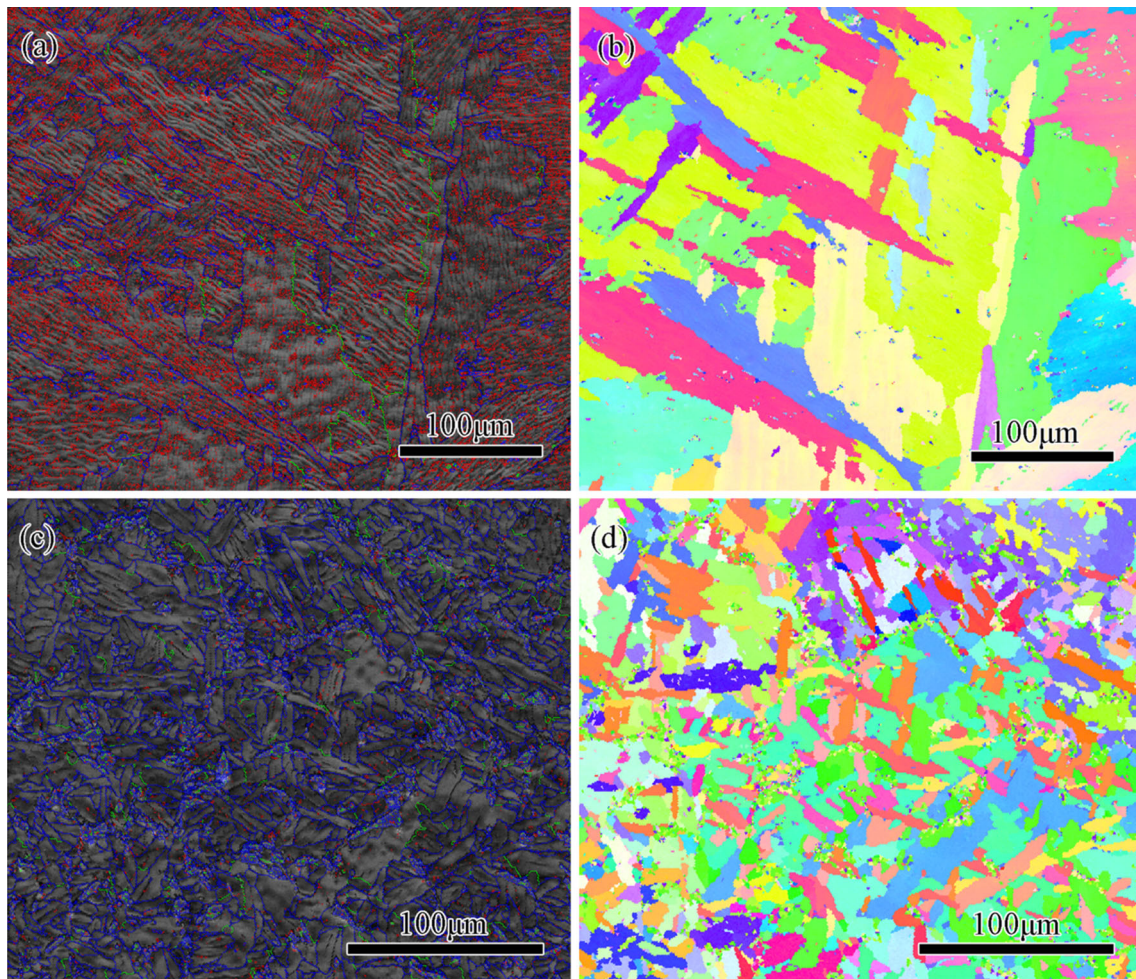


Fig. 3 EBSD maps, **a** grain boundary map of Ti-64, **b** misorientation map of Ti-64, **c** grain boundary map of TMCs, **d** misorientation map of TMCs. Blue lines in **a**, **c** are high-angle ($\theta > 15^\circ$) boundaries,

green lines are middle angle ($15^\circ > \theta > 5^\circ$) boundaries, and red lines are low-angle ($\theta < 5^\circ$) boundaries (Color figure online)

microstructure in which the low-angle boundaries ($<5^\circ$) are dominant. The corresponding misorientation map (Fig. 3b) shows that the parallel α plates have the same orientation and there are several different colonies with different orientation in a prior β grain. In contrast, with the presence of TiB, the whole microstructure, especially the morphology of α phase is greatly changed. In the first place, the low-angle boundaries (Fig. 3c) are less than that in Ti-64 (Fig. 3a). What is more, few α colonies are observed, and the α laths grow into thick and short shape which is more equiaxed. Based on the correlated misorientation analysis (Fig. 3d), the formation of fine and orientated α represented by color variations could be attributed to the TiB whiskers which have various orientations and act as nucleation sites for α phases.

The HTXRD patterns of TMCs are presented in Fig. 4. The position of phase peak in TMCs is changed with the temperature increasing. Increase in lattice parameters due to the thermal expansion is calculated from the peak shift. The calculated results are shown in Table 3, and the maximum error is less than 0.00005 nm in all cases. The thermal expansion coefficient is $9.0 \times 10^{-6}/\text{K}$ for the a-axis and $10.6 \times 10^{-6}/\text{K}$ for the c-axis of the hexagonal unit cell, which correspond very well with the Ref. [20, 21]. For β phase, the thermal expansion coefficient is between

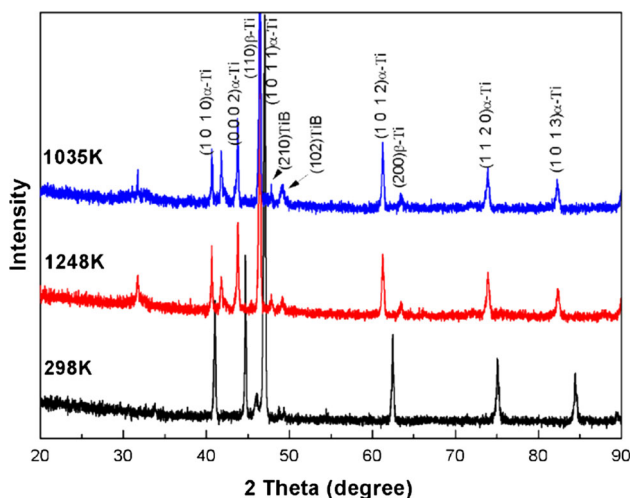


Fig. 4 HTXRD patterns obtained at the temperature of 298, 1248, and 1035 K of TMCs

Table 3 Lattice parameters calculated from HTXRD patterns

Phase	α (hcp)		β (bcc)	TiB		
	X	Z	X	X	Y	Z
298 K (nm)	0.2941	0.4713	0.3326	0.6137	0.3068	0.4369
1248 K (nm)	0.2974	0.4776	0.3392	0.6206	0.3103	0.4691
1308 K (nm)	0.2974	0.4777	0.3393	0.6207	0.3104	0.4692

15.4×10^{-6} and $15.9 \times 10^{-6}/\text{K}$, which is bigger than the thermal expansion coefficient for Ti-64 near room temperature [21]. According to the work of Elmer et al. [21], this is due to a rapid increase in the β phase lattice expansion when the temperature is higher than 1023 K. For TiB phase, the thermal expansion coefficient is between 8.6×10^{-6} and $8.9 \times 10^{-6}/\text{K}$, which correspond with the Ref. [22].

Discussion

The morphology of precipitates in phase transformation is affected by total free energy which is determined by the volume free energy change, elastic energy, and interfacial energy [23, 24]. The free energy during phase transformation is employed to explain the formation of different α morphology in Ti-64 and TMCs. The standard free energy change, ΔG , is expressed as Eq. (1) [24]

$$\Delta G = \frac{4}{3}\pi a^3 R[\Delta G_v + W] + \pi a^2 Y[2 + g(R)], \quad (1)$$

where a is the semi-major axis of an ellipsoidal nucleus, R is the aspect ratio, a/c , c is the semi-minor axis of an ellipsoidal nucleus, ΔG_v is the volume free energy change associated with α nucleation, and Y is the interfacial energy due to the new α phases formation. $g(R)$ is a shape function associated with the aspect ratio R . In this research, $R > 1$ (as shown in Table 2); the function $g(R)$ can be given by [24]

$$g(R) = \frac{2R}{\sqrt{1-R^2}} \sin^{-1}(\sqrt{1-R^2}) \quad (2)$$

W is the elastic strain energy per unit volume of α precipitates formed, which is a function of R [23, 24]

$$W = 2\mu_\alpha \frac{(1+\nu_\alpha)}{(1-\nu_\alpha)} \varepsilon^2 h(R), \quad (3)$$

where ν_α is Poisson's ratio of α , μ_α is the shear modulus of α , E is the elastic modulus, ε is a small quantity [23, 25, 26], and $h(R)$ is a shape function associated with the aspect ratio R . The ratio of shear modulus f is introduced as $f = \mu/\mu_s$, and μ_s is shear modulus of the surrounding. Since $R > 1$, the function $h(R)$ can be given by [23]

$$h(R) = \frac{f(f+3)(1-\nu_\alpha)}{2\{f+(1-2\nu_\alpha)\}}. \quad (4)$$

Schematic drawings of α nucleating at different phases are shown in Fig. 5. In Ti-64, when α phase precipitates directly from β phase (as shown in Fig. 5a), μ_s would be the shear modulus of β phase. The elastic strain energy (W) is obtained as $W_{\alpha/\beta} = 238.5\varepsilon^2 \text{ J/mm}^3$, by substituting the parameters in Table 4 into Eq. (3). But in TMCs, TiB whiskers are believed to act as nucleation sites for α phase (as shown in Fig. 5b). Therefore, the formation of a single

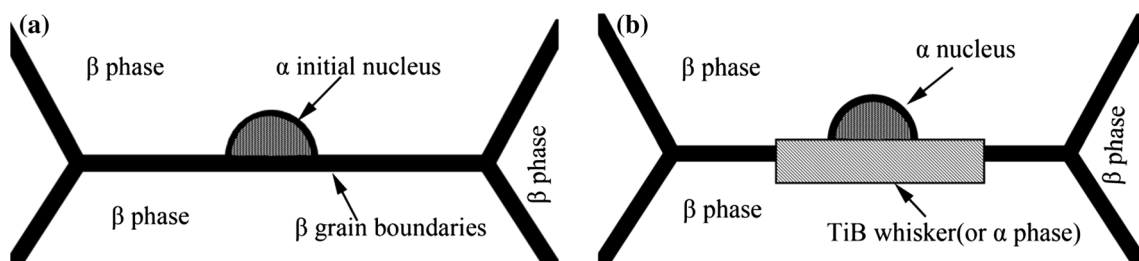


Fig. 5 Schematic diagrams of α nucleating at **a** β grain boundary, **b** TiB whiskers (or grain boundary α phase). The morphology of α initial nucleus is supposed to be hemispherical with $R = 1$

Table 4 Parameters used for calculating free energy

Phase	Elastic modulus (E , GPa)	Poisson's ratio (ν)	shear modulus ($\mu = E/(2 + 2\nu)$, GPa)
α (hcp)	132.2 [27]	0.27 [28]	52
β (bcc)	81.1 [27]	0.27 [28]	31.9
TiB	550 [28]	0.14 [28]	241.2

α nucleus, which is in contact with both TiB phase and β phase, would simultaneously generate two different interfaces, i.e., α /TiB interface and α / β interface. On α /TiB interface, μ_s would be the shear modulus of TiB phase, and $W_{\alpha/\text{TiB}} = 67.8\epsilon^2 \text{ J/mm}^3$, while on the α / β interface, μ_s is the shear modulus of β phase. So when α nucleates at TiB whiskers, the elastic strain energy (W_{TMCs}) can be given as $W_{\text{TMCs}} = W_{\alpha/\text{TiB}}\phi_{\alpha/\text{TiB}} + W_{\alpha/\beta}\phi_{\alpha/\beta}$, (5)

where $\phi_{\alpha/\text{TiB}}$ is the α /TiB interface area fraction which is given as $\phi_{\alpha/\text{TiB}} = S_{\alpha/\text{TiB}}/(S_{\alpha/\text{TiB}} + S_{\alpha/\beta})$, $S_{\alpha/\text{TiB}}$ is the contact area of α phase and TiB, $S_{\alpha/\beta}$ is the contact area of α and β phase, and $\phi_{\alpha/\beta}$ is the α / β interface area fraction which is given as $\phi_{\alpha/\beta} = S_{\alpha/\beta}/(S_{\alpha/\text{TiB}} + S_{\alpha/\beta})$. In the initial stage, the morphology of α nucleus is supposed to be hemispherical with $R = 1$. $S_{\alpha/\text{TiB}} = \pi a_0^2$, $S_{\alpha/\beta} = 2\pi a_0^2$, so, $\phi_{\alpha/\text{TiB}} = 1/3$, and $\phi_{\alpha/\beta} = 2/3$. Substituting the corresponding data to Eq. (5), the elastic strain energy (W_{TMCs}) is obtained as $W_{\text{TMCs}} = 181.6\epsilon^2 \text{ J/mm}^3$. The elastic strain energy reduces to about three quarters of that in Ti-64 due to the presence of TiB whiskers.

The interfacial energy Y consists of the misfit energy Y_m and the energy of the elastic strain field Y_{strain} , which is given by Eq. (6) [29].

$$Y = Y_m + Y_{\text{strain}} = \frac{\mu L_s}{4\pi^2} \left\{ 1 + \gamma - (1 + \gamma^2)^{\frac{1}{2}} \right\} - \frac{\mu L_s \gamma}{4\pi^2} \ln \left\{ 2\gamma(1 + \gamma^2)^{\frac{1}{2}} - 2\gamma^2 \right\}, \quad (6)$$

where L_s is the spacing of lattice of the interface between α precipitates and surrounding and γ is a parameter which is defined as [29]

$$\gamma = 2\pi \frac{L_s \mu_a \mu_b}{\mu p \{ \mu_a (1 - \nu_b) + \mu_b (1 - \nu_a) \}}. \quad (7)$$

The convention used is to denote properties of the precipitates and surroundings above the interface by a and below by b but uses no letters for the properties of the interface itself. Thus, L_a , L_b ; μ_a , μ_b , μ ; and ν_a , ν_b would accordingly designate lattice parameters, shear modulus, and Poisson's ratios, respectively. p is the dislocation spacing, which is defined by Eq. (8) [29].

$$p = (k + 1)L_a = kL_b = \left(k + \frac{1}{2} \right) L_s, \quad (8)$$

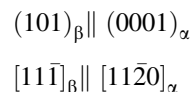
where k is a constant.

The spacing L_s is defined by the Eq. (9), μ is the shear modulus of interface and given by Eq. (10) [29], μ_0 is the value of μ when there is no misfit, and the shear modulus of α phase is used for μ_0 .

$$\frac{2}{L_s} = \frac{1}{L_a} + \frac{1}{L_b} \quad (9)$$

$$\mu = \frac{\mu_0 L_b}{L_a} \quad (10)$$

In Ti-64 alloys, the transformation from β to α generally is governed by the Burgers relationship [13, 30]:



When α precipitates from β phase following the Burgers orientation relationship, the lattice parameters can be calculated by using the data in Table 3. In Ti-64 alloys, the phase transformation temperature is about 1248 K [31]. Thus, $L_a(d(101)_{\beta-\text{Ti}})$ is 0.1696 nm, and $L_b(d(0001)_{\alpha-\text{Ti}})$ is 0.4776 nm. Substituting the corresponding data to Eq. (8) and Eq. (9), the corresponding lattice parameters of Ti-64 can be obtained as $k = 0.551$, $p = 0.263 \text{ nm}$, and $L_s = 0.250 \text{ nm}$.

As reported in previous research [2, 14, 32–35], due to different surface energies, TiB whiskers are liable to grow along the [010] direction and form the whisker shape. It is well known that TiB has (100), (101), and (10 $\bar{1}$) facets as

the exposed faces which are in direct contact with beta phase and are going to be the possible nucleation sites. And the (100) plane of TiB has an orientation relationship with α phase as [34, 35]

$$(100)_{\text{TiB}} \parallel (10\bar{1}0)_{\alpha}$$

In TMCs, the phase transformation temperature is about 1308 K, and the lattice parameters of the interface between TiB and α are calculated by assuming that the α precipitates follow the above orientation relationship. The corresponding lattice parameters are given as $L_a(d(10\bar{1}0)_{\alpha-\text{Ti}}) = 0.2576$ nm, $L_b(d(100)_{\text{TiB}}) = 0.6207$ nm, $k = 0.709$, $p = 0.440$ nm, and $L_s = 0.364$ nm.

By substituting the corresponding data to Eq. (6), the interfacial energies $Y_{\alpha/\beta} = 0.537$ J/m² and $Y_{\alpha/\text{TiB}} = 0.757$ J/m² are obtained, respectively. Similar as W_{TMCs} , when α nucleates at TiB whiskers, the interfacial energy (Y_{TMCs}) can be given as

$$Y_{\text{TMCs}} = Y_{\alpha/\text{TiB}}\phi_{\alpha/\text{TiB}} + Y_{\alpha/\beta}\phi_{\alpha/\beta} \quad (11)$$

Substituting the corresponding data to Eq. (11), the interfacial energy (Y_{TMCs}) is obtained as $Y_{\text{TMCs}} = 0.610$ J/m². The interfacial energy is about 14 % more than that in Ti-64 due to the presence of TiB whiskers.

Substituting Eqs. (2), (3), and (6) into Eq. (1) by using the calculated parameters, the free energy change, ΔG , can be written as

$$\Delta G_{\alpha/\beta} = \frac{4}{3}\pi a^3 R [\Delta G_v + 238.5\varepsilon^2] + \pi a^2 0.537 \left[2 + \frac{2R}{\sqrt{1-R^2}} \sin^{-1}(\sqrt{1-R^2}) \right] \quad (12)$$

$$\Delta G_{\alpha/\text{TiB}} = \frac{4}{3}\pi a^3 R [\Delta G_v + 181.6\varepsilon^2] + \pi a^2 0.610 \left[2 + \frac{2R}{\sqrt{1-R^2}} \sin^{-1}(\sqrt{1-R^2}) \right] \quad (13)$$

As shown in Eqs. (12) and (13), the free energy change (ΔG) depends on the aspect ratio R and the semi-major axes a of α nucleus. Referring to the work of Y. Wang [36], the initial nucleus size a of α phase can be assumed to be 0.25 μm when α phase precipitates from β phase in Ti-64 alloy. The volume free energy change for nucleation α from β (ΔG_v) is about 0.5 kJ/mol [36]. The free energy changes (ΔG) in Ti-64 calculated using Eq. (12) with $\varepsilon^2 = 0.0001, 0.00015, 0.000173, \text{ and } 0.0002$, respectively, are shown in Fig. 6a. It can be seen that, when $\varepsilon^2 = 0.0002$, all calculated values are positive, which reveals that the α phase cannot precipitate from β phase. When $\varepsilon^2 = 0.0001$ and 0.00015, all calculated values are negative, which indicates that the minimum aspect ratio of

α phase would be 1 in this situation. In fact, the minimum aspect ratio of α phase in Ti-64 is 4 as shown in Fig. 1b. However, when $\varepsilon^2 = 0.000173$, the calculated values fit the experimental results well, and the minimum aspect ratio of α phase is 4, which is consistent with experiments results. The free energy changes (ΔG), when TiB acts as nucleation sites for α phase, calculated using Eq. (13) with $\varepsilon^2 = 0.0001, 0.00015, 0.000173, \text{ and } 0.0002$, respectively, are shown in Fig. 6b. It can be indicated that all calculated values are negative, which indicate that the α phase can precipitate in any aspect ratio when the a is 0.25 μm .

The free energy changes (ΔG) in Ti-64 with different initial nucleus size a are calculated as shown in Fig. 6c. It shows that when initial nucleus size a is 0.242 μm , all calculated values are positive, and no α precipitates from β . When initial nucleus size a is 0.25 μm , the minimum aspect ratio R is about 4. While the initial nucleus size a is 0.243 μm , α phase can precipitate from β phase only if the aspect ratio R is bigger than 14, indicating that a small decrease of critical nucleus size (a) results in the big increase of aspect ratio (R).

When TiB acts as nucleation sites for α , the initial nucleus size a can be reduced to 0.1 μm and the minimum R is approximately 3 as seen in Fig. 6d. When β acts as nucleation sites for α , all calculated ΔG values are positive with $a = 0.1$ μm , indicating that α cannot precipitate with such little size in Ti-64 alloys or in α/β boundary. In Ti-64, α phase can precipitate from β phase only if initial nucleus size a is bigger than 0.243 μm , and critical nucleus size is more than two times than that in TMCs.

Figure 6e shows the relationship between the minimum aspect ratio (R_{min}) and the initial nucleus size (a_0). In Ti-64, the β phase acts as nucleation sites for α . When the initial nucleus size (a_0) is bigger than 0.243 μm , α phase will precipitate from β phase. The minimum aspect ratio (R_{min}) will decline sharply with the increase of initial nucleus size (a_0). The increase of initial nucleus needs greater undercooling; however, the decrease of transformation temperature will limit the nucleus growth. In this research, the alloys are cooled in ceramic shell which has the thermal insulation effects and reduces the cooling rate, and the small initial nucleus size (a_0) has advantage in α phase precipitation. Therefore, the initial nucleus size (a_0) of α phase is about 0.25 μm and the aspect ratio of α phase is between 4 and 29 in Ti-64 alloys as shown in Fig. 1b. In TMCs, TiB whiskers would act as α phase nucleation sites. The minimum aspect ratio (R_{min}) is about 3 when the initial nucleus size (a_0) is 0.1 μm as shown in Fig. 6e. As the initial nucleus size (a_0) grows up to 0.12 μm , the minimum aspect ratio (R_{min}) decreases to 1. The TMCs are also cooled in ceramic shell, the α phases will prefer to grow up in small initial nucleus size, and most of aspect ratio is between 2 and 4 in TMCs as shown in Fig. 1d.

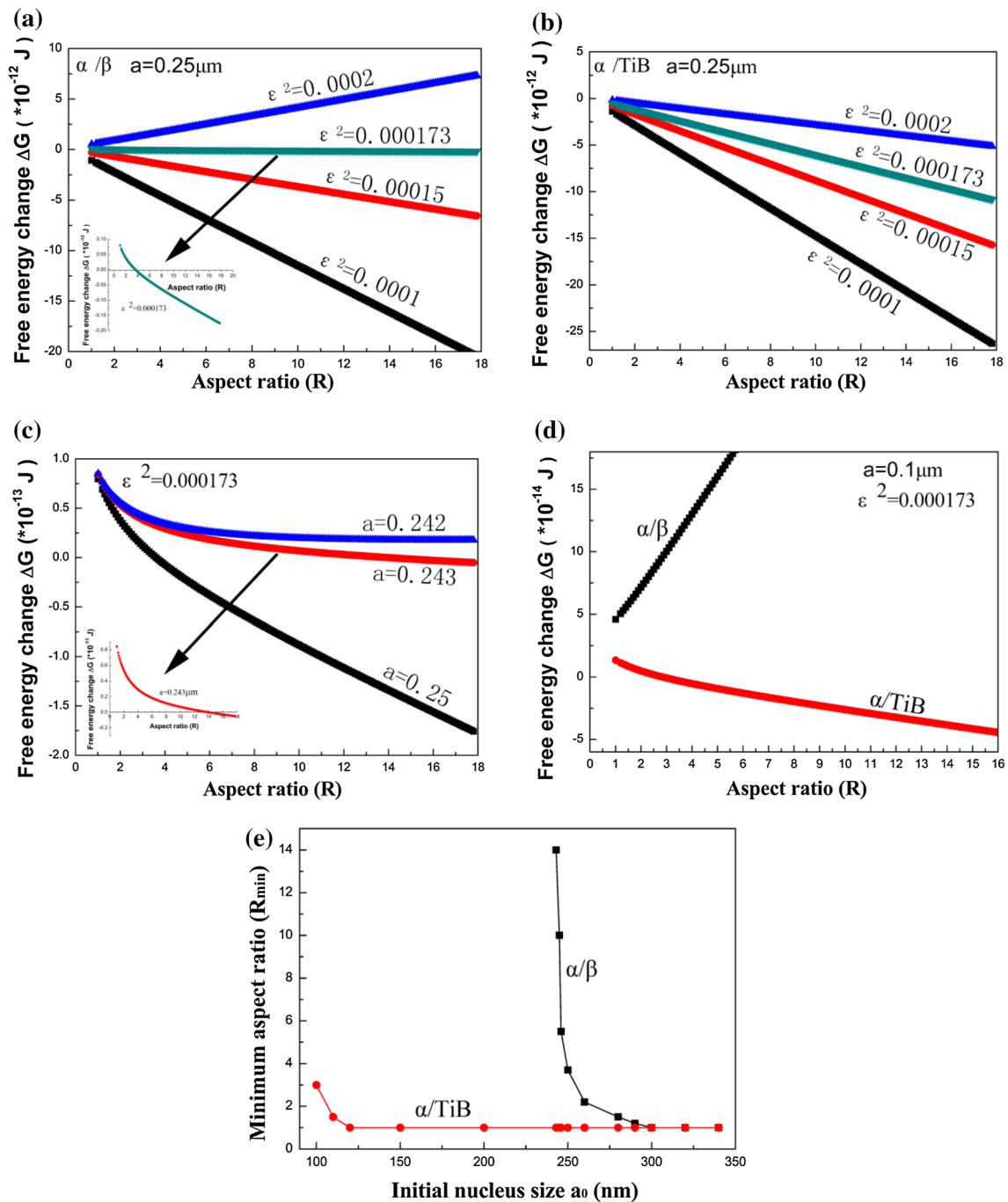


Fig. 6 Variation of ΔG with R for α precipitated in Ti-64 or TMCs. **a** The variation of ΔG with R in Ti-64 calculated using Eq. (12) with $\varepsilon^2 = 0.0001, 0.00015, 0.000173, \text{ and } 0.0002$. **b** The variation of ΔG with R , when TiB acts as nucleation sites for α phase, calculated using Eq. (13) with $\varepsilon^2 = 0.0001, 0.00015, 0.000173, \text{ and } 0.0002$.

c The variation of ΔG with R in Ti-64 with different initial nucleus size a . **d** The variation of ΔG with R when $a = 0.1\mu\text{m}$. **e** The variation of the minimum aspect ratio (R_{\min}) with the initial nucleus size (a_0) which the R_{\min} is defined as the aspect ratio R when the ΔG is just <0 with a certain initial nucleus size (a_0)

In Ti-64 alloys, the α laths can also nucleate from the grain boundary α . On the α/α interface, u_s would be the shear modulus of α phase, and $W_{\alpha/\alpha} = 180.9\varepsilon^2 \text{ J/mm}^3$. Similar as nucleating from TiB whiskers, on the other

interface, α nucleus is contacted with β phase, so the elastic strain energy ($W_{\alpha/\text{boundary}\alpha}$) can be given as

$$W_{\alpha/\text{boundary}\alpha} = W_{\alpha/\alpha}\phi_{\alpha/\alpha} + W_{\alpha/\beta}\phi_{\alpha/\beta} \tag{14}$$

So, the elastic strain energy ($W_{\alpha/\text{boundary } \alpha}$) is dropping by 8 % from $238.5\epsilon^2 \text{ J/mm}^3$ to $219.3\epsilon^2 \text{ J/mm}^3$.

When α laths nucleate from the grain boundary alpha, there is a coupled interface between α laths and grain boundary alpha. So the interfacial energy ($Y_{\alpha/\text{boundary } \alpha}$) can be given as

$$Y_{\alpha/\text{boundary } \alpha} = Y_{\alpha/\beta} \phi_{\alpha/\beta} \quad (15)$$

Substituting the corresponding data to Eq. (15), the interfacial energy ($Y_{\alpha/\text{boundary } \alpha}$) is dropping by more than 33 % from 0.537 to 0.358 J/m^2 .

On the one hand, the reduction of the elastic strain energy and interfacial energy which is the transformation resistance will promote the precipitation of α phase. On the other hand, due to sharply reduced interfacial energy, the α phase prefers to grow into lamellar structure with high aspect ratio.

In general, due to the existence of TiB, the interfacial energy of α/TiB is about 14 % more than that in Ti-64 alloys, and the elastic strain energy declines to about three quarters of that in Ti-64 alloys. When TiB whiskers act as the nucleation sites of α precipitations, the α phase is easy to precipitate in a very small size initially and then tends to be more equiaxed with an average aspect ratio of 3.4 in TMCs.

Conclusions

The addition of B_4C to Ti-64 modifies the phase transformation behavior of the Ti-64 alloy and also alters its microstructures. In this paper, the effects of B_4C additions on the microstructures and morphology change of α phase of TMCs prepared by investment casting are investigated. The following conclusions can be drawn from this study:

- (1) With the addition of B_4C , the average primary β grain is refined, the widmanstatten structure is eliminated, the number of low-angle boundaries between α phases decreases, and the morphology of α phase tends to be more equiaxed.
- (2) With addition of 0.48 wt% B_4C , the average aspect ratio of α phases declines from 13.8 to 3.4, which is attributed to the increase of the interfacial energy and decrease of elastic strain energy of α phases when TiB settles in the grain boundary and acts as the α nucleation site. When TiB acts as nucleation site for α , the critical nucleus size (a) could be reduced to $0.1 \mu\text{m}$ with the minimum aspect ratio $R = 3$, indicating that the α phase could precipitate in a very small size initially and then tends to be more equiaxed. However, when β acts as nucleation site for α , the initial nucleus size is supposed to be larger than $0.243 \mu\text{m}$, a small decrease of critical

nucleus size results in the big increase of aspect ratio (R), and critical nucleus size is more than two times than that in α/TiB boundary.

Acknowledgements We would like to acknowledge the financial support provided by the National Nature Science Foundation of China under Grant No.: 51371114, the 973 Program under Grant No.: 2012CB619600, the China Postdoctoral Science Foundation under Grant No.: 2014M550235, No.: 2014M561467, and the Shanghai Postdoctoral Sustentation Fund under Grant No. 14R21410900.

References

1. Lu JQ, Qin JN, Lu WJ, Zhang D, Hou HL, Li ZQ (2009) Effect of hydrogen on microstructure and high temperature deformation of (TiB + TiC)/Ti-6Al-4V composite. *Mater Sci Eng A* 500:1–7
2. Lu WJ, Zhang D, Zhang XN et al (2001) Microstructure and tensile properties of in situ synthesized (TiBw + TiCp)/Ti6242 composites. *J Mater Sci* 36:3707–3714. doi:10.1023/a:1017917631855
3. Ni DR, Geng L, Zhang J, Zheng ZZ (2008) Fabrication and tensile properties of in situ TiBw and TiCp hybrid-reinforced titanium matrix composites based on Ti-B4C-C. *Mater Sci Eng A* 478:291–296. doi:10.1016/j.msea.2007.06.004
4. Wang JH, Guo XL, Xiao L et al (2014) Effect of B4C on the microstructure and mechanical properties of as-cast TiB + TiC/TiC4 composites. *Acta Metallurgica Sinica* 27:205–210
5. Qin YL, Geng L, Ni DR (2011) Dry sliding wear behavior of extruded titanium matrix composite reinforced by in situ TiB whisker and TiC particle. *J Mater Sci* 46:4980–4985. doi:10.1007/s10853-011-5415-x
6. Morsi K, Patel VV (2007) Processing and properties of titanium-titanium boride (TiBw) matrix composites—a review. *J Mater Sci* 42:2037–2047
7. Li YG, Xiao L, Lu WJ, Qin JN, Zhang D (2008) Creep rupture property of in situ synthesized (TiB + La_2O_3)/Ti composite. *Mater Sci Eng A* 488:415–419
8. Ma FC, Lu WJ, Qin JN, Zhang D (2006) Strengthening mechanisms of carbon element in in situ TiC/Ti-1100 composites. *J Mater Sci* 41:5395–5398
9. Ranganath S, Vijayakumar M, Subrahmanyam J (1992) Combustion-assisted synthesis of Ti-TiB-TiC composite via the casting route. *Mater Sci Eng A* 149:253–257
10. Zhang XN, Lü WJ, Zhang D, Wu RJ, Bian YJ, Fang PW (1999) In situ technique for synthesizing (TiB + TiC)/Ti composites. *Scripta Mater* 41:39–46
11. Tamirisakandala S, Bhat RB, Tiley JS, Miracle DB (2005) Grain refinement of cast titanium alloys via trace boron addition. *Scripta Mater* 53:1421–1426
12. Ferri OM, Ebel T, Bormann R (2011) The influence of a small boron addition on the microstructure and mechanical properties of Ti-6Al-4V Fabricated by metal injection moulding. *Adv Eng Mater* 13:436–447
13. Hill D, Banerjee R, Huber D, Tiley J, Fraser HL (2005) Formation of equiaxed alpha in TiB reinforced Ti alloy composites. *Scripta Mater* 52:387–392
14. Lu WJ, Zhang D, Zhang XN, Guo SL, Wui RJ (2001) Growth mechanism of reinforcements in in situ synthesized (TiB + TiC)/Ti composites. *Trans Nonferr Met Soc China* 11:67–71
15. Cheng TT (2000) The mechanism of grain refinement in TiAl alloys by boron addition—an alternative hypothesis. *Intermetallics* 8:29–37

16. De Barros MI, Rats D, Vandembulcke L, Farges G (1999) Influence of internal diffusion barriers on carbon diffusion in pure titanium and Ti–6Al–4V during diamond deposition. *Diam Relat Mater* 8:1022–1032
17. Cadoff I, Nielsen JP (1953) Titanium-carbon phase diagram. *J Met* 5:1564
18. Sen I, Tamirisakandala S, Miracle DB, Ramamurty U (2007) Microstructural effects on the mechanical behavior of B-modified Ti–6Al–4V alloys. *Acta Mater* 55:4983–4993
19. Nandwana P, Nag S, Hill D, Tiley J, Fraser HL, Banerjee R (2012) On the correlation between the morphology of α and its crystallographic orientation relationship with TiB and β in boron-containing Ti–5Al–5Mo–5V–3Cr–0.5 Fe alloy. *Scripta Mater* 66:598–601
20. Spreadborough J, Christian JW (1959) The measurement of the lattice expansions and debye temperatures of titanium and silver by X-ray methods. *Proc Phys Soc* 74:609–615
21. Elmer JW, Palmer TA, Babu SS, Specht ED (2005) In situ observations of lattice expansion and transformation rates of α and β phases in Ti–6Al–4V. *Mater Sci Eng A* 391:104–113
22. Gorsse S, Chaminade JP, Le Petitcorps Y (1998) In situ preparation of titanium base composites reinforced by TiB single crystals using a powder metallurgy technique. *Compos A* 29:1229–1234
23. Kato M, Fujii T, Onaka S (1996) Elastic strain energies of sphere, plate and needle inclusions. *Mater Sci Eng A* 211:95–103
24. Lee JK, Barnett DM, Aaronson HI (1977) The elastic strain energy of coherent ellipsoidal precipitates in anisotropic crystalline solids. *Metall Trans A* 8:963–970
25. Onaka S, Fujii T, Kato M (1995) The elastic strain energy of a coherent inclusion with deviatoric misfit strains. *Mech Mater* 20:329–336
26. Kato M, Fujii T, Onaka S (1996) Elastic state and orientation of needle-shaped inclusions. *Acta Mater* 44:1263–1269
27. Sen I, Ramamurty U (2010) Elastic modulus of Ti–6Al–4V–xB alloys with B up to 0.55 wt%. *Scripta Mater* 62:37–40
28. Fan Z, Miodownik AP, Chandrasekaran L, Ward-Close M (1994) The Young's moduli of in situ Ti/TiB composites obtained by rapid solidification processing. *J Mater Sci* 29:1127–1134
29. JH Van Der Merwe (1963) Crystal interfaces. Part I. Semi-infinite crystals. *J Appl Phys* 34:117
30. Stanford N, Bate PS (2004) Crystallographic variant selection in Ti–6Al–4V. *Acta Mater* 52:5215–5224
31. Seshacharyulu T, Medeiros SC, Morgan JT, Malas JC, Frazier WG, Prasad YVRK (2000) Hot deformation and microstructural damage mechanisms in extra-low interstitial (ELI) grade Ti–6Al–4V. *Mater Sci Eng A* 279:289–299
32. Lu WJ, Zhang D, Zhang XN, Wu RJ, Sakata T, Mori H (2001) Microstructural characterization of TiB in in situ synthesized titanium matrix composites prepared by common casting technique. *J Alloy Compd* 327:240–247
33. Lu WJ, Xiao L, Geng K, Qin JN, Zhang D (2008) Growth mechanism of in situ synthesized TiBw in titanium matrix composites prepared by common casting technique. *Mater Charact* 59:912–919. doi:10.1016/j.matchar.2007.07.016
34. Hyman ME, McCullough C, Valencia JJ, Levi CG, Mehrabian R (1989) Microstructure evolution in TiAl alloys with B additions: conventional solidification. *Metall Trans A* 20:1847–1859. doi:10.1007/bf02663215
35. Feng HB, Zhou Y, Jia DC, Meng QC, Rao JC (2006) Growth mechanism of in situ TiB whiskers in spark plasma sintered TiB/Ti metal matrix composites. *Cryst Growth Des* 6:1626–1630
36. Shi RP, Wang YZ (2013) Variant selection during α precipitation in Ti–6Al–4V under the influence of local stress—A simulation study. *Acta Mater* 61:6006–6024